ACS APPLIED MATERIALS & INTERFACES

Research Article

www.acsami.org

Mesostructured Nanomagnetic Polyhedral Oligomeric Silsesquioxanes (POSS) Incorporated with Dithiol Organic Anchors for Multiple Pollutants Capturing in Wastewater

Hai-Bo He,*[,†] Bin Li,[†] Jun-Ping Dong,[†] Yun-Yi Lei,[†] Tian-Lin Wang,[†] Qiong-Wei Yu,[‡] Yu-Qi Feng,*[,‡] and You-Bao Sun[§]

[†]Department of Chemistry, Shanghai University, Shanghai, 200444, P.R. China

[‡]Key Laboratory of Analytical Chemistry for Biology and Medicine (Ministry of Education), Department of Chemistry, Wuhan University, Wuhan, 430072, P.R. China

[§]Shimadzu (China) Co., Ltd., Shanghai Branch, Shanghai, 200052, P.R. China

Supporting Information

ABSTRACT: A functionalizable organosiliceous hybrid magnetic material was facilely constructed by surface polymerization of octavinyl polyhedral oligomeric silsesquioxane (POSS) on the Fe_3O_4 nanoparticles. The resultant Fe_3O_4@POSS was identified as a mesoporous architecture with an average particle diameter of 20 nm and high specific surface area up to 653.59 $m^2\ g^{-1}$. After it was tethered with an organic chain containing dithiol via thiol−ene addition reaction, the ultimate material (Fe_3O_4@POSS-SH) still have moderate specific area (224.20 $m^2\ g^{-1}$) with almost identical porous morphology. It turns out to be a convenient, efficient single adsorbent for simultaneous elimination of inorganic heavy metal ions and organic dyes in simulate multicomponent wastewater at ambient temperature. The Fe_3O_4@POSS-SH nanoparticles can be readily withdrawn from aqueous solutions within a few seconds under moderate magnetic field and exhibit good stability in strong acid and alkaline aqueous matrices. Contaminants-loaded Fe_3O_4@POSS-SH can be easily regenerated with either methanol−acetic acid (for organic dyes) or hydrochloric acid (for heavy metal ions) under ultrasonication. The renewed one keeps appreciable adsorption capability toward both heavy metal ions and organic dyes, the removal rate for any of the pollutants exceeds 92% to simulate wastewater with multiple pollutants after repeated use for 5 cycles. Beyond the environmental remediation function, thanks to the pendant vinyl groups, the Fe_3O_4@POSS derived materials rationally integrating distinct or versatile functions could be envisaged and consequently a wide variety of applications may emerge.

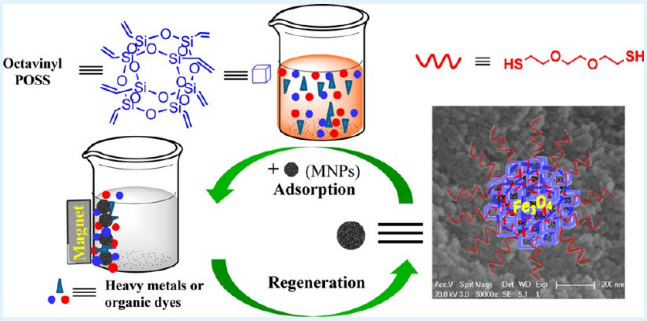

KEYWORDS: *multiple pollutants capture, mesostructure, thiol-functionalized, nanomagnetic POSS adsorbent*

1. INTRODUCTION

Water contamination due to various organic and inorganic pollutants remains a serious environmental and public problem. Heavy metal ions and organic dyes are major environmentally harmful water pollutants commonly associated with industrial and agricultural effluents. Heavy metal ions, such as mercury, lead, silver are nonbiodegradable and can be accumulated in the environment and living tissues, causing various diseases and disorders of living organisms even at a trace level.[1−8] The synthetic cationic dyestuffs, such as malachite green (MG) and rhodamine B (RB), can produce adverse health effects for both human beings and wildlife because of their carcinogenesis, mutagenesis, teratogenesis, and chronic toxicity.[9−14] Therefore, separation and remediation technologies are highly needed to reduce the residual pollutants contents below the acceptable threshold values by existing regulations before exposure. Sorption technique is one of the most effective and economical way that has been developed for this purpose.[2,7,11,15]

Recently the silica based mesoporous inorganic/organic hybrid materials are particular attractive as adsorbents for environmental remediation.[15−17] Indeed, one can expect its high performance for sequestering toxic substances from water samples, due to the large surface areas, well-defined pore structures, and tunable surface properties. Unfortunately, mesoporous materials usually exist in superfine powdered form with microsized particles, which are difficult to be separated from solution after batch adsorption experiments and easy to cause secondary pollution. As a development in this area, numerous studies have been devoted to the preparation of

Received: June 3, 2013
Accepted: July 30, 2013
Published: July 30, 2013

novel adsorbing materials by combination of mesoporous silica with magnetic separation.[7,18−24] Imparting magnetism to adsorbents afford a rapid and economic approach to remove the toxic compounds from large-volume samples by applying an appropriate magnetic field. Attempts to derive functionalized adsorbents based on magnetic mesoporous silica are undoubtedly of great potential application prospect. More recently, the core/shell-type magnetic mesoporous silica nanocomposites have been the subject of extensive research concerning water treatment as they exhibit high stability and varied functionality.[25] Typically, such materials can be synthesized by a combination of surfactant-based self-assembly and sol−gel processes,[26] and the functionality involves highly susceptible silylation or co-condensation routes, thereby suffering from rather expensive sacrificial templates (surfactants such as cetyltrimethylammonium bromide, block copolymers, such as F127) to generate mesostructure and tedious procedures (such as the synthesis of silanes with expected functional groups because of the lack of commercially available silanes monomers, and/or drying of the solvents, repeating hydrolysis and silylation cycles) to obtain desirable functionalities.[15,18,19] Additionally, the previously reported functionalized mesoporous silica adsorbents, whether magnetic or not, prevailed in the accumulation of single pollutants from wastewater.[1,7,10,15,19,21] These constitute real restrictions in extensive applications for real-world environmental cleanup process. Regarding the industrial and commercial requirements, it is ideal if efficient mesostructured nanomagnetic materials with multifunctionalities can be achieved by a facile, universal, and economic synthetic approach.

Among the various innovative approaches for building porous materials with specific functionality and structure, the stepwise assembly of predefined nanoscale building blocks is an intriguing strategy that can be finely designed and synthesized by tuning the primary building blocks.[27,28] Polyhedral oligomeric silsesquioxanes (POSS) are recently regarded as ideal building blocks for constructing organic−inorganic hybrid materials. A typical polyhedral oligomeric silsesquioxane (POSS) molecule possesses a cubic rigid (T_8) structure represented by the formula $R_8Si_8O_{12}$, where the central inorganic core (Si_8O_{12}) is functionalized with organic moieties (R) at each of the eight vertices.[29,30] Microporous/mesoporous materials based on POSS precursors have been prepared by various chemical routes including hydrosilation methods,[31] thermolysis,[32] copper-mediated coupling,[33] and Schiff base chemistry.[34] In particular, Nischang[35,36] pioneered a facile, single-step process by using octavinyl POSS as the sole building blocks in polymerization to construct versatile, high-surface-area, hierarchically structured hybrid materials, therein the nanoporosity of the derived materials could be readily tuned by the use of a relatively inexpensive (in comparison to surfactants and block copolymers) binary porogenic solvent mixture (THF or PEG), and tailorability of the interface properties by functionalization of the residual vinyl groups via thiol−ene addition was also demonstrated.

Inspired by the examples presented above, the fabrication of magnetic mesoporous hybrid materials from POSS building blocks appears indeed desirable. Herein, we proposed a facile route to prepare POSS based magnetic organosilica nanoparticles (Fe_3O_4@POSS) via a radically initiated polymerization. Rather than grafting of the methacryloxypropylheptaisobutyl−POSS/methacrylate based block copolymers from magnetic nanoparticles as recently reported,[37] the primary rationale for our approach is self-assembling of the sole building blocks of octavinyl POSS to generate mesostructured and functionalizable hybrid layers. Copolymerization occurred on vinyl groups is a versatile synthetic tool for controlling the functionality, and, therefore, tailoring of the chemical, physical, and mechanical properties of materials. Since there are abundant residual vinyl groups resulting from POSS in case of the Fe_3O_4@POSS, it is adaptable to a wide range of functional monomers to realized derived materials with new properties. For example, it is well-known that numerous vinyl monomers can be employed for polymerization according to the free-radical polymerization principle, the atom-transfer radical polymerization (ATRP) is tolerant toward various halogenated reagents.[38] Extensive research have been carried out in the field of thiol−ene "click" addition, for the advantages such as simple, high efficiency, and high-yield.[39,40] It should be emphasized that these synthetic strategies can be carried out under mild reaction conditions. Taking the aforementioned various modification methods into account, it is highly anticipated to derive a wide range of porous structured magnetic materials with controllable functionalities, thereby extensive applications covering environmental remediation, sample pretreatment, drug delivery, catalysis, and magnetic resonance imaging are foreseeable.

As a preliminary exploitation, the modification of Fe_3O_4@POSS was implemented by introducing dithiol organic anchors via thiol−ene addition reaction. From the environmental point of view, thiol is a well-known group for the entrapment of heavy metal ions,[7,15,21,22,41] while the hydrophobicity resulting from self-assembled POSS layer[29,35] is compatible with the treatment of organic pollutants. Therefore, the removal of multiple pollutants from the wastewater by the Fe_3O_4@POSS-SH adsorbent was demonstrated in our present work. To the best of our knowledge, this is the first work on manufacturing POSS based mesoporous nanomagnetic organosilica, as well as employing it as a single adsorbent to deal with multiple pollutants from wastewater.

2. EXPERIMENTAL SECTION

2.1. Materials. Ferric chloride ($FeCl_3·6H_2O$), ferrous chloride ($FeCl_2·4H_2O$), aqueous ammonia solution (25%), acrylic acid, lead nitrate ($Pb(NO_3)_2$), silver nitrate ($AgNO_3$), and mercuric nitrate ($Hg(NO_3)_2·H_2O$) were purchased from Sinopharm Chemical Reagent Co., Ltd.(China). Octavinyloctasilasesquioxane and 2,2′-azobisobutyronitrile (AIBN) were obtained from Aladdin Chemistry Co., Ltd. 3,6-Dioxa-1,8-octanedithiol, malachite green, and rhodamine B were got from TCI(Shanghai) Development Co., Ltd. AIBN was recrystallized in ethanol before use. All other reagents were of analytical purity and were used as received without further purification. Double distilled water was used throughout the experiments.

2.2. Preparation of Fe_3O_4@POSS-SH. Bare Fe_3O_4 magnetic nanoparticles were prepared by chemical coprecipitation according to the reported procedure.[42] Acrylic acid (AA) was coated on the surface of Fe_3O_4 to produce AA-Fe_3O_4. Magnetic nanoparticles (2.00 g) were dispersed in 100 mL of acrylic acid aqueous solution, the pH of which was adjusted to 5.50 with alkaline solution, followed by stirring at 85 °C for 1 h under N_2 gas protection. The sediment was separated with an external magnet. After it was washed by distilled water and ethanol for several times, the double bond coated composites were dried in vacuum.

The Fe_3O_4@POSS was synthesized as follows: POSS (400 mg) was dissolved in binary solvent mixture of 2700 μL of THF and 535 μL of PEG 200. Then 255 mg of AA-Fe_3O_4 was added to the suspension and was ultrasonically mixed for 5 min. The polymerization was initiated by the addition of 96 mg of AIBN at 60 °C. After 24 h, the as-prepared

Scheme 1. Schematic Representation of the Route for Synthesis of Fe_3O_4@POSS-SH

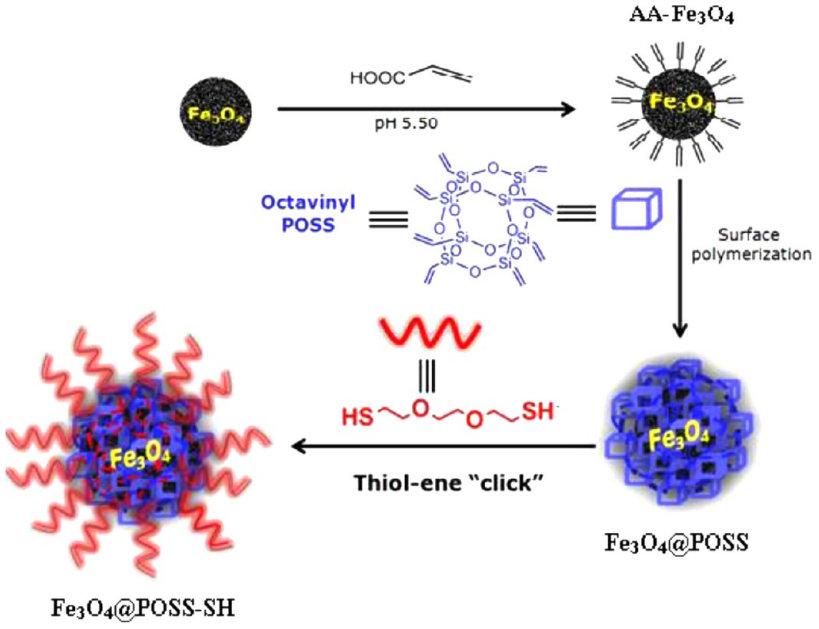

Fe_3O_4@POSS composites were subjected to extraction with THF in a Soxhlet apparatus until the eluent was transparent before drying or use.

The Fe_3O_4@POSS-SH was fabricated by modification of Fe_3O_4@POSS particles with 3,6-dioxa-1,8-octanedithiol through thiol−ene addition reaction. In a typical batch, 100 mg of Fe_3O_4@POSS and 350 μL of dithiol were mixed adequately in 20 mL of ethanol in a flask fitted with a condenser. Thereafter, 50 mg of AIBN was added into the mixture, and the reaction was carried out at 60 °C refluxing for 12 h with stirring and bubbling with nitrogen stream throughout the procedure. Finally, the resultants were magnetically collected and then purified by repeating washing, decantation, and resuspension in water and ethanol. The as-prepared adsorbent was dried in a vacuum oven overnight before the adsorption of pollutants. Scheme 1 illustrated the synthesis process of Fe_3O_4@POSS-SH.

2.3. Characterization. The scanning electron microscopy (SEM) was used to observe the surface morphologies and dimensions of Fe_3O_4, Fe_3O_4@POSS and Fe_3O_4@POSS-SH samples, and the SEM images were taken with an S-4800 field emission scanning electron microscope (FE-SEM, Hitachi, Japan) at an accelerating voltage of 20 kV with an energy-dispersive X-ray (EDX) spectroscopy. Fourier-transform infrared (FT-IR) spectra scanned over the range of 400−4000 cm^{-1} with KBr slice on a Nicolet Avatar 370 spectrometer (Nicolet Thermo, U.S.A.) were employed to examine the chemical nature of the synthesized composites. The C, H, and S elemental contents analysis were performed on an EA3000 analyzer (Euro Vector, Italy).The nitrogen adsorption/desorption isotherms were measured by using an ASAP 2020 N_2 adsorption and desorption analyzer (Micromeritics Co., Ltd., U.S.A.). Surface area was calculated using the Brunauer−Emmett−Teller (BET) equation from the adsorption isotherms in the relative pressure range of 0.06−0.15. Pore diameters were determined from the desorption branch of the isotherm using the Barrett−Joyner−Halenda (BJH) method. The total pore volume was calculated at a relative pressure of P/P_0 above 0.99. The samples were degassed under vacuum at 120 °C for 5 h prior to measuring at −196 °C. Wide angle X-ray powder diffraction patterns (XRD) of the magnetic products were obtained at room temperature on a D-MAX/IIA rotation anode X-ray diffractometer (Rigaku Corporation, Japan) equipped with Cu Kα radiation (λ = 1.5406 Å) at a scan rate of 4° 2θ min^{-1} from 10° to 70° (2θ). Magnetic properties were analyzed using a vibrating sample magnetometer (VSM, Lakeshore Model-7410, U.S.A.).

2.4. Adsorption Experiments. To assess the adsorption efficiency, static adsorption tests were done by taking malachite green, rhodamine B, lead nitrate, silver nitrate, and mercuric nitrate as probes. Water samples were prepared by spiking water with known amounts of heavy metal salts or organic dyes. The simulated wastewater consisted of malachite green, silver nitrate, mercuric nitrate with an individual concentration of 10 mg L^{-1}. Various aqueous solutions (10 mL) were, respectively, shaken together with desired amounts of Fe_3O_4@POSS-SH for 1 h at room temperarue. After the adsorbents had been isolated by an external magnet, the supernatant was transferred to instrumental analysis.

UV−vis absorption spectra of organic dyes were collected on an SP-2500 spectrum instrument (Shanghai Spectrum Co., Ltd., China). The concentrations of heavy metal ions were measured by inductively coupled plasma atomic emission spectrometer (ICP-AES) of ICPE-9000 (Shimadzu, Japan).

The initial concentrations of heavy metal ions and organic dyes at diverse levels were selected to yield adsorption isotherms. The specific amount adsorbed onto Fe_3O_4@POSS-SH was calculated based on the following formula:[43]

$$Q_e = \frac{(C_0 - C_e) \times V}{M} \quad (1)$$

where Q_e (mg g^{-1}) is the equilibrium adsorption capacities, C_0 (mg L^{-1}) is the initial concentration, C_e (mg L^{-1}) is the equilibrium concentration, V (L) is the volume of the aqueous solution and M (g) is the mass of the adsorbent used.

To optimize the usage of adsorbents, it is important to analyze the adsorption equilibrium data. The well-known Langmuir isotherm and Freundlich isotherm were applied to evaluate the adsorption behavior of probe solutes on Fe_3O_4@POSS-SH adsorbent.

The Langmuir model concerns monolayer adsorption onto a homogeneous surface and can be written as follows:[11,17]

$$\frac{C_e}{q_e} = \frac{1}{q_{max} K_L} + \frac{C_e}{q_{max}} \quad (2)$$

where C_e (mg L^{-1}) is the equilibrium concentration of solute, q_e (mg g^{-1}) is the equilibrium adsorption capacity of adsorbent, q_{max} (mg g^{-1}) is the saturated adsorption amount of adsorbent, ans K_L is the Langmuir adsorption constant.

dx.doi.org/10.1021/am402137c | ACS Appl. Mater. Interfaces 2013, 5, 8058−8066

The Freundlich model assumes multilayer adsorption occurs on a heterogeneous surface and the linearized equation can be expressed as follows:[20,43]

$$\log q_e = \log K_F + \frac{1}{n}\log C_e \quad (3)$$

where C_e (mg L^{-1}) is the equilibrium concentration of solute, q_e (mg g^{-1}) is the equilibrium adsorption capacity of adsorbent, K_F (L g^{-1}), and n are Freundlich isotherm constants, which refer to the capacity and intensity of the adsorption, respectively.

3. RESULTS AND DISCUSSION

3.1. Synthesis and Characterization of the Materials.

In the present work, iron oxide magnetic nanoparticles (MNPs) were prepared by coprecipitation method, which is simple and yields high production,[44] thus facilitating the massive applications of such materials among the following approaches.

To improve dispersibility and promote functionality of iron oxide particle chunks, acrylic acid (AA) was coated on the nanoparticles via Lewis acid−base and hydrogen bonding interaction between −COOH and iron oxide surface.[41,45] In the presence of free radicals, the vinyl groups on the surface of AA-Fe_3O_4 may act as spacers to anchor POSS entities and contribute to construct polymeric coated magnetic materials, though polymerization and initation will proceed also anywhere else in this complex mixture. The porosity of polymer can be readily tailored free from surfactants by using binary porogens of THF and PEG 200. An inherent consequence of the polymerization of a multifunctional vinyl monomeric species is the existence of numerous residual vinyl groups,[35] thus 3,6-dioxa-1,8-octanedithiol can be incorporated to the surface of Fe_3O_4@POSS particles by thiol−ene addition reaction.

The typical SEM images of Fe_3O_4, Fe_3O_4@POSS and Fe_3O_4@POSS-SH are shown in Figure 1 at 80 000 × magnification. Figure 1a indicates that the pristine Fe_3O_4 particles are nearly spherical in appearance with an average diameter of 10 nm. Similar rough polymeric coating with irregular cavities appears on the surface of Fe_3O_4@POSS and Fe_3O_4@POSS-SH; however, a growth in the average particle size about 20−30 nm were observed in Figure 1b and 1c.Table 1 summarized the contents of various elements on the surface of Fe_3O_4@POSS and Fe_3O_4@POSS-SH particles obtaining from SEM-EDX spectra (see the Supporting Information, Figure S1). It is apparent that the surface of the two POSS derived MNPs is dominated by Si, indicating an effective surface coating on bare Fe_3O_4. The Fe_3O_4@POSS-SH is rich in S but rare in Fe, suggesting that the magnetic property is further protected by the self-assembled POSS layer during the "thiol−ene" reaction process.

To gain further insights into the chemical changes associated with the reactions shown in Scheme 1, FT-IR spectroscopic measurements were also performed. As expected, in Figure 2, all the spectra hold a clearly visible characteristic peak of Fe_3O_4 at 580 cm^{-1}. Figure 2b displays that after chemical modified with AA, the adsorption peak of Fe−OH at 1635 cm^{-1} in Figure 2a overlaps with the peak at 1639 cm^{-1} relating to the stretching vibration of the C═C bond in acrylic acid. The load of AA in AA-Fe_3O_4 was determined to be 0.21 mmol g^{-1} according to the content of carbon element (0.763 wt %, 0.64 mmol g^{-1}). Figure 2c and Figure 2d show strong Si−O−Si stretching vibration bands at 1110 cm^{-1}, which is the typical absorption peak of the silsesquioxane inorganic framework (Si−O−Si), implying the successful attachment of POSS onto the AA-Fe_3O_4. In Figure 2c, the peaks at 3050, 1600, 1410, and

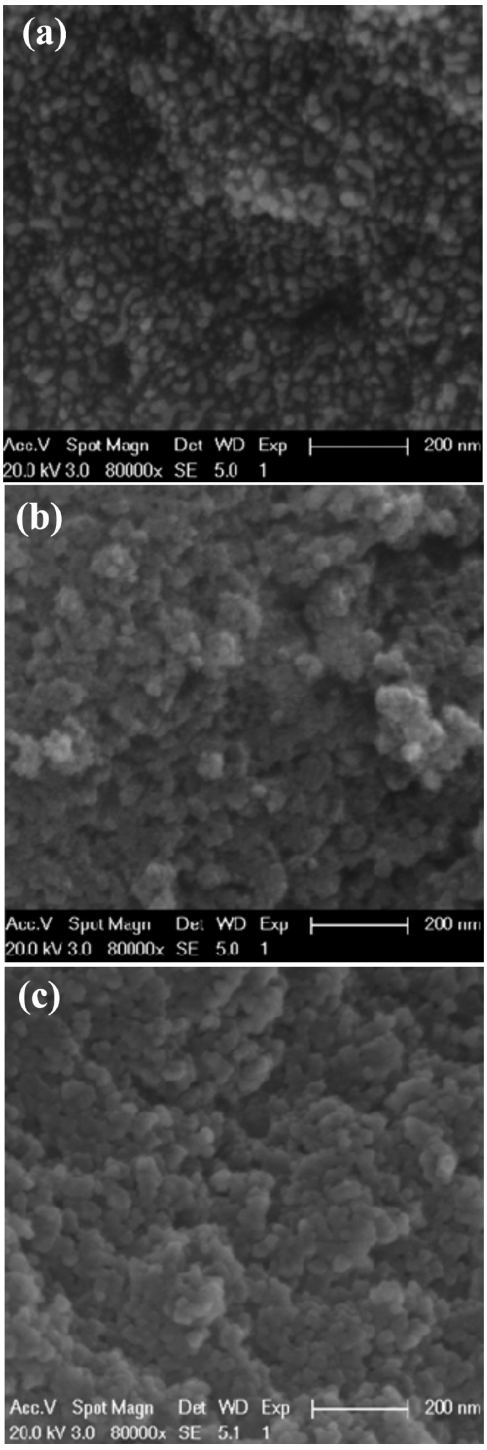

Figure 1. Representative scanning electron micrographs of (a) Fe_3O_4, (b) Fe_3O_4@POSS, and (c) Fe_3O_4@POSS-SH.

1275 cm^{-1} are characteristic of the residual vinyl groups of POSS. After chemically grafted the 3,6-dioxa-1,8-octanedithiol by thiol−ene addition reaction, the intensities of these peaks decrease, while those of alkyl bands around 2930 ($\upsilon^{as}_{CH_2}$) and 2850 cm^{-1} ($\upsilon^{s}_{CH_2}$) increase significantly as shown in Figure 2d. No obvious peak of δ_{SH} at 2580 cm^{-1} was found in Figure 2d because it is difficult to detect the stretching vibration due to the weak dipoles.[20] Nevertheless, the content of sulfur in the Fe_3O_4@POSS-SH was about 10 mmol g^{-1} calculating from

dx.doi.org/10.1021/am402137c | ACS Appl. Mater. Interfaces 2013, 5, 8058−8066

Table 1. Weight and Atomic Percents of Various Elements on the Surface of Fe_3O_4@POSS and Fe_3O_4@POSS-SH from the Analysis of EDX

	Fe_3O_4@POSS		Fe_3O_4@POSS-SH	
element	weight percent (%)	atomic percent (%)	weight percent (%)	atomic percent (%)
C	30.03	46.35	31.76	46.62
O	26.77	31.01	26.79	29.51
Si	25.32	16.71	24.31	15.26
Fe	17.88	5.94	3.47	1.09
S			13.67	7.51

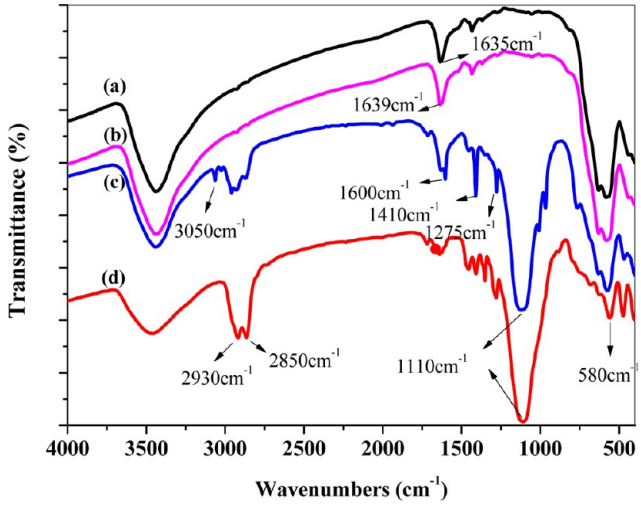

Figure 2. FT-IR spectra of (a) Fe_3O_4, (b) AA-Fe_3O_4, (c) Fe_3O_4@POSS, and (d) Fe_3O_4@POSS-SH.

elemental analysis, further evidencing the occurrence of thiol–ene addition reaction on the surface of Fe_3O_4@POSS. Elemental analyses of C, H, and S are listed in Table S1 (see the Supporting Information, Table S1).

Figure 3a and 3b display the nitrogen sorption isotherms and the corresponding pore size distribution curves of Fe_3O_4@POSS and Fe_3O_4@POSS-SH, respectively. A type IV isotherm with steep hysteresis loop at relative pressure (P/P_0) of 0.45 can be observed, indicating that the two materials have mesoporous structures that originate from the highly cross-linked POSS units. The Fe_3O_4@POSS was proved to have high specific surface area of 653.59 $m^2\ g^{-1}$ and narrow pore size distribution with an average diameter of 4.56 nm. The corresponding data of Fe_3O_4@POSS-SH are 224.20 $m^2\ g^{-1}$ and 4.45 nm, respectively. It is worthwhile to note that after modification by thiols, there is little variation in pore size but notable shrink in BET surface area and pore volume (from 0.70 to 0.28 $cm^3\ g^{-1}$), implying the thiol groups would be partially introduced into the interior space of the meso-structrued pores. Although the dimension of "pore window" was almost unaffected, the pore "cavity and wall" may be blocked in a great extent during functionalization. This is similar to what has been observed by Hao et.al as previously reported.[46]

The crystal phases of magnetic products are investigated by XRD analysis. Figure 3c shows the similar XRD diffraction patterns in which six diffraction peaks (220, 311, 400, 422, 511, and 440) are seen and indexed to the spinal phases for iron oxides. A broad peak with 2θ about centered at 20° was observed in so-called Fe_3O_4@POSS, and Fe_3O_4@POSS-SH (Figure 3c), indicating the formation of amorphous silica polymers on nanocomposites. The results revealed that chemical modification of the iron oxide nanoparticls did not make significant changes in the phase property of Fe_3O_4.

Sufficient magnetic properties are necessary for practical applications of magnetic materials in aqueous solutions. Field dependent magnetization measurements on the samples were conducted to study their magnetic behaviors. Figure 3d shows VSM magnetization curves of Fe_3O_4, Fe_3O_4@POSS, and Fe_3O_4@POSS-SH at room temperature. Clearly, the magnetic hysteresis loop curves exhibit neither coercivity nor remanence, indicating that these nanocomposites are superparamagnetic. Maximun saturation magnetizations of Fe_3O_4, Fe_3O_4@POSS, and Fe_3O_4@POSS-SH are measured at 53.80, 29.82, and 14.29 emu g^{-1}, respectively. The decrease in the magnetic strength of nanocomposites results from the POSS coating. As can be observed from Figure S3 (see the Supporting Information), the saturation magnetization of Fe_3O_4@POSS-SH is still enough for magnetic separation in a very short time by applying a magnet.

3.2. Adsorption Behaviors of the POSS-Based MNPs.

Herein, the octavinyl POSS possesses a cubic rigid (T_8) structure with the central inorganic core (Si_8O_{12}) is functionalized with organic vinyl moieties at each of the eight vertices, both the Si–O core and the vinyl groups provide hydrophobic environment for nonpolar compounds.[29,35] After a polymerization step, the resulted Fe_3O_4@POSS has mesoporous structure coupled with high surface area and subsequently high-density POSS layer with hydrophobic property, which should be an ideal adsorbent for the capture of organic compounds such as water-soluble organic dyes. Thiol is well-known to have a great affinity toward many metal ions, such as Ag^+, Hg^{2+}, Pb^{2+}, and so on. Accordingly, the as-prepared Fe_3O_4@POSS-SH is highly anticipated to integrate the adsorption functions originated from POSS and thiol, thus enables effective elimination of multiple pollutants in water treatment. In the following study, several environmentally harmful organic dyes and heavy metal ions commonly associated with industrial and agricultural effluents were chosen to explore the adsorption performance of Fe_3O_4@POSS-SH. For comparison, the adsorption performance of Fe_3O_4@POSS was also investigated.

As expected, the Fe_3O_4@POSS exhibits good adsorb ability for the tested organic dyes as demonstrated in Figure 4a and 4b, suggesting the strong binding interactions between the organic dyes and the high surface area porous hybrid coating stemming from cross-linked POSS. It should be pointed out that the uptake of such organic dyes becomes more efficient when the Fe_3O_4@POSS was modified with dithiol organic chain. Typically, 5 mg of Fe_3O_4@POSS-SH could remove almost 100% of the malachite green and 96% of the rhodamine B in an individual water sample with the initial concentration of 10 mg L^{-1} (data gathered in Figure 4). As demonstrated by vivid photographs in inset of Figure 4a and Figure 4b, the color in the aqueous solutions of free dyes has markedly faded after adsorption, and the analytes-loaded nanoparticle adsorbent could be fast collected by a magnet within several seconds. Identically, as displayed in Figure 4c in terms of Pb^{2+}, Hg^{2+}, and Ag^+, although the Fe_3O_4@POSS can remove these heavy metal ions to some extent because of the nanoporous hybrid chemisty from the self-assembled POSS, the material was found to have much better adsorption performance after the introduction of thiol groups, which are principally attributed to the strong

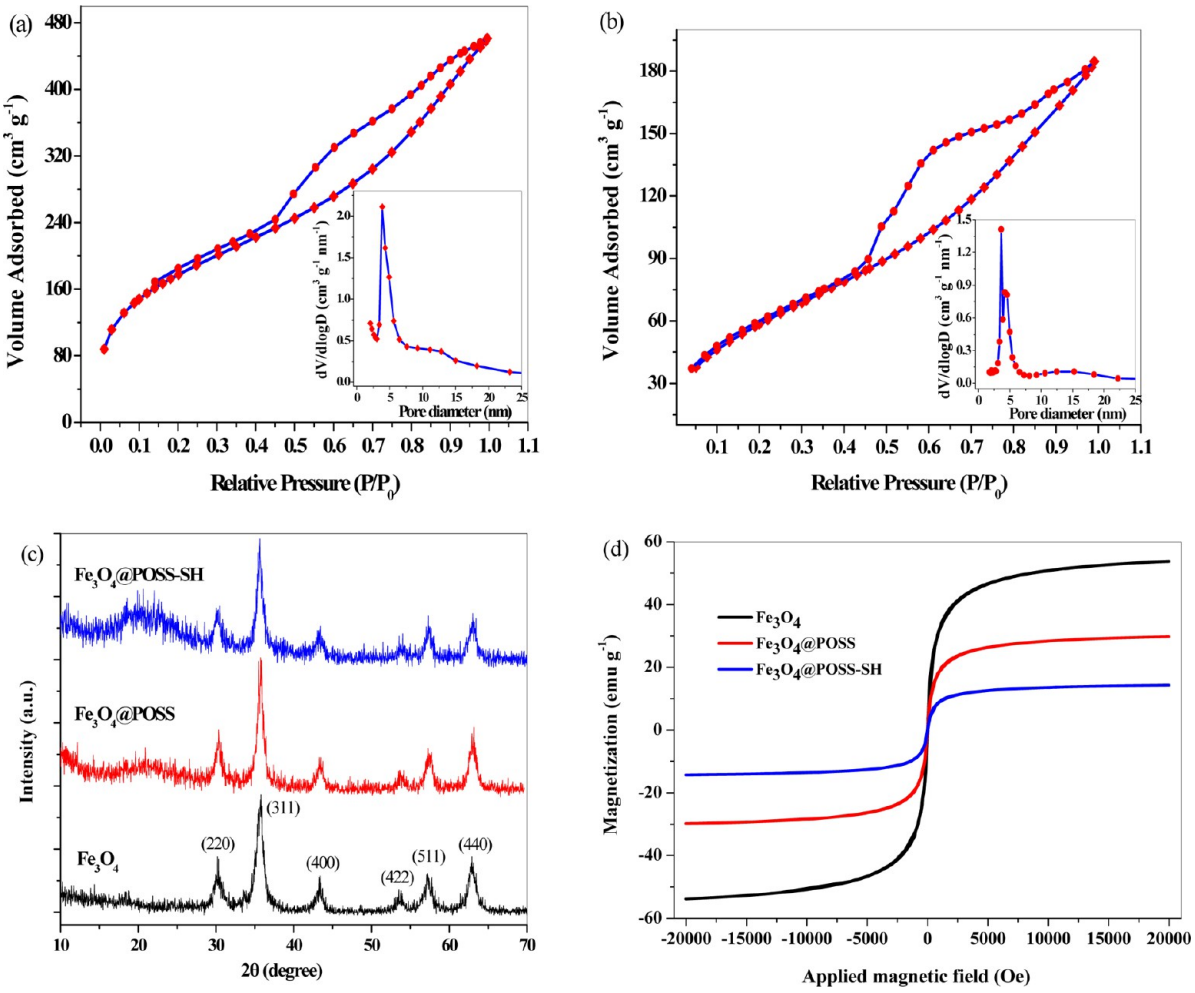

Figure 3. Nitrogen adsorption−desorption isotherms of (a) Fe_3O_4@POSS and (b) Fe_3O_4@POSS-SH (the insets are corresponding pore size distribution curves), (c) XRD patterns, and (d) VSM magnetization curves of Fe_3O_4, Fe_3O_4@POSS, and Fe_3O_4@POSS-SH.

chelating affinity of free thiol groups toward heavy metal ions. As a matter of fact, the sulfur and oxygen atoms existing in Fe_3O_4@POSS-SH are also likely to coordinate with metal ions. The Fe_3O_4@POSS-SH as a consequent potential adsorbent was investigated thoroughly in the following study.

To investigate the effect of pH on the adsorption performance for dyes and metal ions, the Fe_3O_4@POSS-SH material was mixed with the solution of an individual pollutant at a concentration of 10 mg L^{-1} in the range pH range of 3−9 (adjusted by 0.1 M NaOH and HNO_3). The results are summarized in Figure 5. Evidently, the adsorption of both dyes and metal ions were pH-dependent.

As shown in Figure 5a, at lower pH (3−6) the adsorption capacity of MG and RB both increased as the pH increased, then kept almost constant for MG with further increasing pH, the RB however reached a maximum at pH 6−7. MG and RB are cationic dyes, which have positive charge in general aqueous solution.[13,47] At lower pH, the strong protonation of the −SH groups[4,7] on the material caused electrostatic repulsion with the positively charged dyes, thus lead to the decreased adsorption capacity as pH decreased. The adsorption capacity of MG changed a little in the pH range of 6−9 and the highest adsorption capacity of RB obtained around pH 6−7, implying that the hydrophobic interaction plays a key role between the material and such dyes. When pH is higher than 7, the deprotonation of amine and carboxylic groups in rhodamine B gives rise to a negatively charged molecule,[14] whose adsorption in turn dropped due to the weakening of the hydrophobic interaction.

In Figure 5b, the adsorption capacities of metal ions increased as the pH increased from 4 to 7 and presented a maximum around pH 7, then decreased with increasing pH in the range of 7−9. The results are mainly attributed to the following reasons:[4,7] (1) at lower pH, the −SH groups are pronated, thus diminishing their chelating ability to metal ions and (2) alkaline conditions hinder the adsorption of heavy metals because of formation of stable hydroxyl complexes or hydroxides.

It should be emphasized that the pH of natural water is mostly around 7, moreover, in view of the superiority of adsorption performance on both dyes and metal ions at this pH according to the above results, the adsorption tests were conducted without pH adjustment throughout the following adsorption experiment, thereby facilitating the real-life wastewater treatment due to less procedure of sample handling.

The adsorption isotherms in Figure S2 (see the Supporting Information) demonstrate a positive functional relationship between the adsorption capacity of the Fe_3O_4@POSS-SH and the equilibrium concentration of pollutants. The fitting isotherm parameters are listed in Table 2. For metal ions, the higher correlation coefficients (R_L^2) of the linearized Langmuir equation than these of Freundlich equation (R_F^2) indicate that

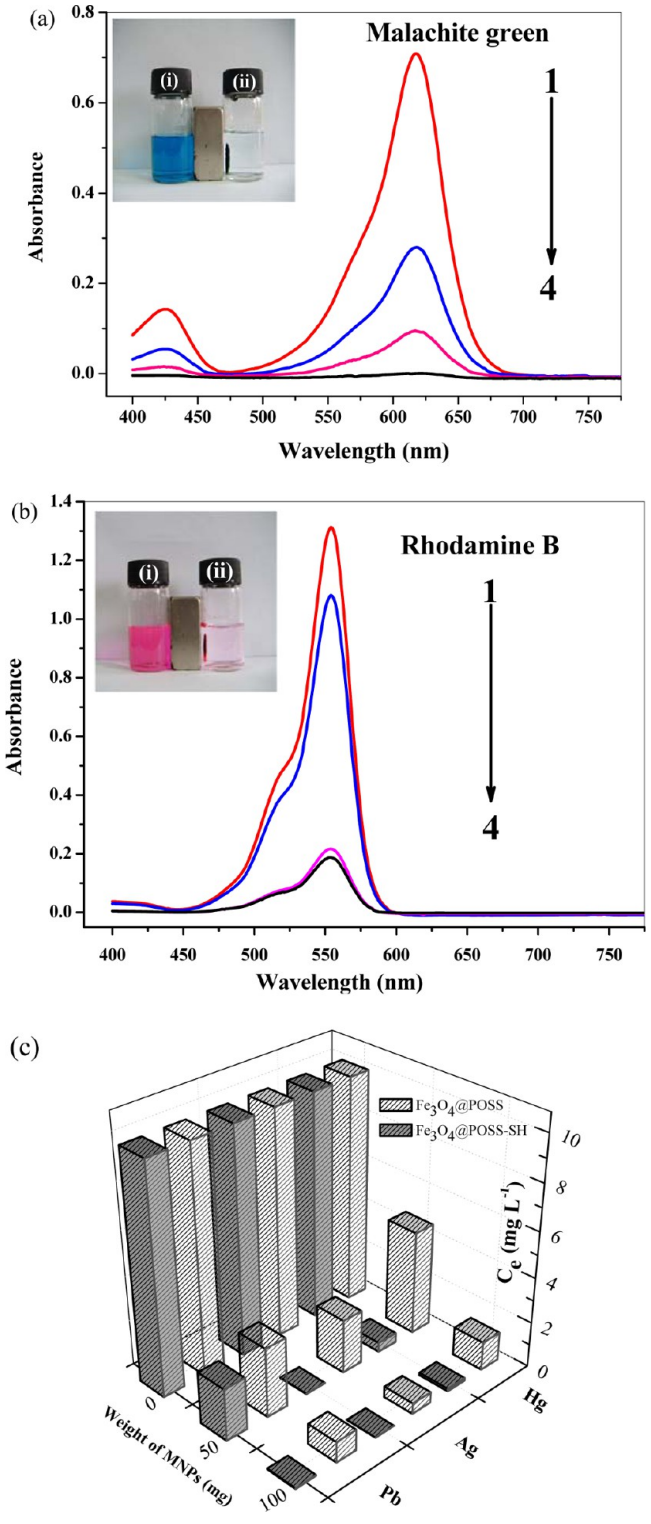

Figure 4. Comparative absorption spectra of (a) malachite green, (b) rhodamine B, and (c) comparisons between the adsorption of heavy metal ions by different amounts of Fe_3O_4@POSS and Fe_3O_4@POSS-SH nanoparticles. Curves 1−4 stand for the dye solutions treated with 1 mg of Fe_3O_4@POSS, 1 mg of Fe_3O_4@POSS-SH, 5 mg of Fe_3O_4@POSS, and 5 mg of Fe_3O_4@POSS-SH, respectively. The insets are photographs of (i) initial solutions (10 mg $L^{-1}$of dye) and (ii) dye solutions after adsorption by the Fe_3O_4@POSS-SH left under the magnet for 10 s.

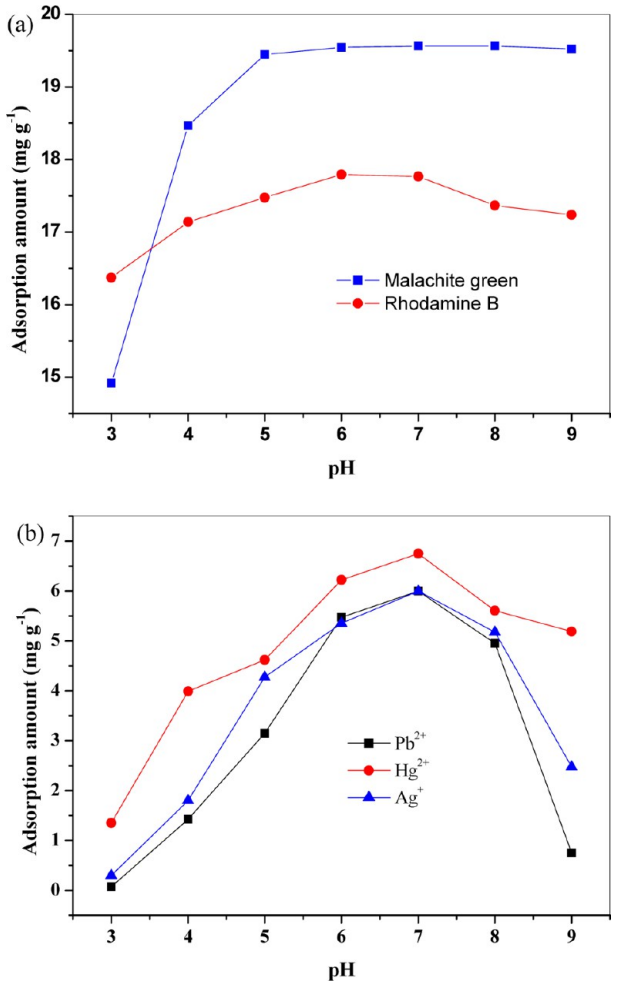

Figure 5. Effect of pH on the adsorption amounts of (a) dyes and (b) heavy metal ions by Fe_3O_4@POSS-SH (initial concentration of each pollutant = 10 mg L^{-1}, adsorbent dosage = 5 mg/10 mL for dyes, adsorbent dosage = 20 mg/15 mL for metal ions, room temperature).

Table 2. Isotherm Parameters for the Adsorption of Pollutants onto Fe_3O_4@POSS-SH

	Langmuir isotherm			Freundlich isotherm		
pollutants	q_{max} (mg g^{-1})	K_L (L mg^{-1})	R_L^2	K_F (L g^{-1})	n	R_F^2
Pb^{2+}	90.90	0.042	0.995	18.74	3.33	0.976
Hg^{2+}	99.80	0.051	0.996	23.74	3.57	0.988
Ag^{+}	100.00	0.051	0.997	23.47	3.73	0.959
Malachite green	111.01	0.23	0.991	37.98	3.94	0.998
Rhodamine B	142.05	0.089	0.986	20.18	2.22	0.996

Langmuir model can better fit to the experimental results. The adsorption behaviors of malachite green and rhodamine B dyes on the Fe_3O_4@POSS-SH, however, comply with the multilayer type of Freundlich isotherm based on the fitting results. A detailed comparison with other magnetic mesoporous silica adsorbents that used for the adsorption of metal ions and organic pollutants (Table S2 in Supporting Information) indicates that, the as-prepared Fe_3O_4@POSS-SH has some advantages in terms of surfactant free for mesoporous formation, facile operation in functionalization and comparable adsorption capacities of metal ions and dye. Moreover, it has

dx.doi.org/10.1021/am402137c | ACS Appl. Mater. Interfaces 2013, 5, 8058−8066

the potential as a single adsorbent for the simultaneou removal of multiple pollutants.

3.3. Purification of Simulated Wastewater and Regeneration of Fe_3O_4@POSS-SH. The designed Fe_3O_4@POSS-SH as a single adsorbent for the removal of multicomponent pollutants in wastewater is delineated as below. Simulated wastewater was prepared by malachite green, silver nitrate, and mercuric nitrate with the same concentrations of 10 mg L^{-1}. After purification by 100 mg of adsorbent, the residual Hg^{2+} and Ag^{+} is 0.15 and 0.052 mg L^{-1}, respectively, while the solution turns to be completely colorless and no dye is monitored, meaning that the Fe_3O_4@POSS-SH can clear almost all the hazardous materials (98.5% of Hg^{2+}, 99.5% of Ag^{+}, and 100% of dye). These results further throw light on the superior purification ability of the novel adsorbent for practical wastewater with complicated components.

Furthermore, the stability of Fe_3O_4@POSS-SH in aqueous phases was assessed by contacting with various corrosive solutions (Figure S3 in the Supporting Information). Naked Fe_3O_4 particles were observed easily digested by strong acids as liquids in left bottles in Supporting Information Figure S3c and d present yellow-green color obviously. The Fe_3O_4@POSS-SH, however, was estimated rather resistant to strong acid and basic conditions, as no visible change for transparent liquid with the Fe_3O_4@POSS-SH immersed for 48 h (right bottles in Supporting Inforamtion Figure S3c and d). The results are certifications of a complete coating for Fe_3O_4 by POSS as proposed. Actually, POSS as a building block for constructing functional molecules and nanometric materials shows significantly high thermal and chemical stability.[29]

The "simulated wastewater contaminated" material was then regenerated according to the literatures[7,10] with a little procedure modification: after treated with 5 × 2 mL of methanol–acetic acid (95:5, v/v) and 5 × 2 mL of 1 mol L^{-1} HCl in sequence under untrasonic (Note: 2.0 mL of each elution solution for 10 min in every time, eluted 5 times in every cycles), the desorption efficiency was almost 100% for MG meanwhile over 98% for metal ions when the fresh adsorbent used for the first time. Thus methanol–acetic acid (95:5, v/v) and 1 mol L^{-1} HCl solutions with the above procedure were chosen for respectively releasing of MG and metal ions from the material in repeated cycles of regeneration. The extent of Fe leaching from Fe_3O_4@POSS-SH during regeneration was also measured quantitatively. The respective eluate from the first 3 cycles was collected and used for ICP-AES analysis. As listed in Supporting Information Table S3, only a small proportion of Fe (<1.5 wt %) was detected in the eluate even under ultrasonic in strong acid aqueous solution. Such low leaching of Fe from Fe_3O_4@POSS-SH would also result in little sacrifice of its magnetism. Therefore, the Fe_3O_4@POSS-SH featured with the rigid silica cube shell is believed to be excellently stable in natural water matrices and wastewater. And its regeneration becomes more feasible by desorption of the pollutants even under extreme conditions.

The reusability of the regenerated material was tested by using for removal of pollutants in the simulated wastewater. As depicted in Figure 6, the removal efficiency for the simulate wastewater dropped slightly in the subsequent regeneration-reuse cycles. As the renewed one kept desirable removal efficiency (at least 92%) after reuse in 5 cycles, the as-prepared Fe_3O_4@POSS-SH is believe to have good reusability. This would allow economic and practical operation in relation to wastewater purification, as well as monitoring analysis, where

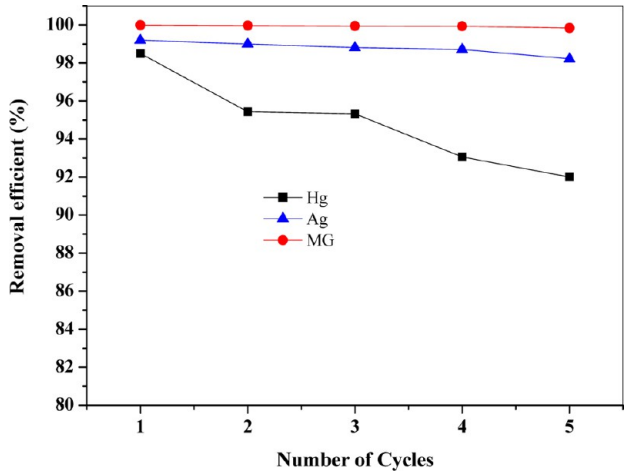

Figure 6. Removal efficiency of Fe_3O_4@POSS-SH for Hg^{2+} and Ag^{+}, malachite green in simulated wastewater in repeated adsorption–desorption cycles (in every cycle, initial concentration of each pollutant = 10 mg L^{-1}, adsorbent dosage = 100 mg/10 mL, pH = 7, temperature = 25 °C).

noxious contaminations are present at (ultra)low concentration. The present merits of the material may be ascribe to its nanoporous structure with high BET surface area and tailored functionality via thiol–ene addition reaction, the inherent unique inorganic/organic hybrid framework of POSS should also not be ignored.

4. CONCLUSIONS

Here, we endowed the functionalizable POSS with magnetism by a facile polymerization step, then mercapto functionalized magnetic porous adsorbent of nanometer size (Fe_3O_4@POSS-SH) was successfully achieved via the thiol–ene addition reaction. The obtained thiol tagged magnetic inorganic/organic hybrid material turns out to be an ideal single adsorbent for purifying wastewater coexisting with inorganic heavy metal ions and organic dyes at room temperature. Furthermore, the proposed adsorbent can be easily recovered and the renewed one bears desirable ability to remove the contaminants. In view of the good capture/release efficiency, the nanoadsorbent has the potential for enrichment of such analytes from complex matrices in trace analysis. More than that, this highly flexible route concerning POSS, as for well-tailored functionalized magnetic porous materials may emerge for various applications in which anticipated multifunctions, as well as high surface areas are required.

■ ASSOCIATED CONTENT

Ⓢ Supporting Information

Elemental analysis, EDX spectra of Fe_3O_4@POSS and Fe_3O_4@POSS-SH, adsorption isotherms of metal ions and organic dyes, photos of erosion results for Fe_3O_4 and Fe_3O_4@POSS-SH, and leaking of Fe in eluate. This material is available free of charge via the Internet at http://pubs.acs.org.

■ AUTHOR INFORMATION

Corresponding Author

*H.-B.E.: E-mail hbhe2006@shu.edu.cn; fax +86-21-66134594; tel +86-21-66132930. Y.-Q.F.: E-mail yqfeng@whu.edu.cn; fax +86-27-68755595; tel +86-27-68755595

Notes

The authors declare no competing financial interest.

■ ACKNOWLEDGMENTS

This work was funded by the National Science Foundation of China (Grants20905046 and 21005057). The authors gratefully thank the Instrumental Analysis & Research Center of Shanghai University for instrumentation.

■ REFERENCES

(1) Zhong, L. X.; Peng, X. W.; Yang, D.; Sun, R. C. *J. Agric. Food Chem.* **2012**, *60*, 5621−5628.
(2) Yantasee, W.; Rutledge, R. D.; Chouyyok, W.; Sukwarotwat, V.; Orr, G.; Warner, C. L.; Warner, M. G.; Fryxell, G. E.; Wiacek, R. J.; Timchalk, C.; Addleman, R. S. *ACS Appl. Mater. Interfaces* **2010**, *2*, 2749−2758.
(3) He, F.; Wang, W.; Moon, J. W.; Howe, J.; Pierce, E. M.; Liang, L. Y. *ACS Appl. Mater. Interfaces* **2012**, *4*, 4373−4379.
(4) Zhang, C.; Sui, J. H.; Li, J.; Tang, Y. L.; Cai, W. *Chem. Eng. J.* **2012**, *210*, 45−52.
(5) Liu, J. S.; Du, X. Z. *J. Mater. Chem.* **2011**, *21*, 6981−6987.
(6) Wang, C.; Tao, S. Y.; Wei, W.; Meng, C. G.; Liu, F. Y.; Han, M. *J. Mater. Chem.* **2010**, *20*, 4635−4641.
(7) Li, G. L.; Zhao, Z. S.; Liu, J. Y.; Jiang, G. B. *J. Hazard. Mater.* **2011**, *192*, 277−283.
(8) Qu, Q. S.; Gu, Q.; Gu, Z. L.; Shen, Y. Q.; Wang, C. Y.; Hu, X. Y. *Colloids Surf., A* **2012**, *415*, 41−46.
(9) Soylak, M.; Unsal, Y. E.; Yilmaz, E.; Tuzen, M. *Food Chem. Toxicol.* **2011**, *49*, 1796−1799.
(10) Liu, R.; Hei, W.; He, P.; Li, Z. *J. Chromatogr. B* **2011**, *879*, 2416−2422.
(11) Zhou, L.; Gao, C.; Xu, W. J. *ACS Appl. Mater. Interfaces* **2010**, *2*, 1483−1491.
(12) Gupta, V. K.; Mohan, D.; Sharma, S.; Sharma, M. *Sep. Sci. Technol.* **2000**, *35*, 2097−2113.
(13) Sun, H. M.; Cao, L. Y.; Lu, L. H. *Nano Res.* **2011**, *4*, 550−562.
(14) Gao, H. C.; Sun, Y. M.; Zhou, J. J.; Xu, R.; Duan, H. W. *ACS Appl. Mater. Interfaces* **2013**, *5*, 425−432.
(15) Walcarius, A.; Mercier, L. *J. Mater. Chem.* **2010**, *20*, 4478−4511.
(16) Stein, A.; Melde, B. J.; Schroden, R. C. *Adv. Mater.* **2000**, *12*, 1403−1419.
(17) Shi, W. P.; Tao, S. Y.; Yu, Y. X.; Wang, Y. C.; Ma, W. *J. Mater. Chem.* **2011**, *21*, 15567−15574.
(18) Li, W.; Zhao, D. Y. *Adv. Mater.* **2013**, *25*, 142−149.
(19) Lu, A. H.; Salabas, E. L.; Schüth, F. *Angew. Chem., Int. Ed.* **2007**, *46*, 1222−1244.
(20) Tao, S. Y.; Wang, C.; Ma, W.; Wu, S.; Meng, C. G. *Microporous Mesoporous Mater.* **2012**, *147*, 295−301.
(21) Wang, Y. Y.; Li, B.; Zhang, L. M.; Li, P.; Wang, L. L.; Zhang, J. *Langmuir* **2012**, *28*, 1657−1662.
(22) Hakami, O.; Zhang, Y.; Banks, C. J. *Water Res.* **2012**, *46*, 3913−3922.
(23) Li, X. S.; Zhu, G. T.; Luo, Y. B.; Yuan, B. F.; Feng, Y. Q. *TrAC, Trends Anal. Chem.* **2013**, *45*, 233−247.
(24) Chen, L. G.; Wang, T.; Tong, J. *TrAC, Trends Anal. Chem.* **2011**, *30*, 1095−1108.
(25) Liu, J.; Qiao, S. Z.; Hu, Q. H.; Lu, G. Q. *Small* **2011**, *7*, 425−443.
(26) Deng, Y. H.; Wang, C. C.; Hu, J. H.; Yang, W. L.; Fu, S. K. *Colloids Surf., A* **2005**, *262*, 87−93.
(27) Sanchez, C.; Soler-Illia, G. J. d. A. A.; Ribot, F.; Lalot, T.; Mayer, C. R.; Cabuil, V. *Chem. Mater.* **2001**, *13*, 3061−3083.
(28) Murugavel, R.; Walawalkar, M. G.; Dan, M.; Roesky, H. W.; R.Rao, C. N. *Acc. Chem. Res.* **2004**, *37*, 763−774.
(29) Tanaka, K.; Chujo, Y. *J. Mater. Chem.* **2012**, *22*, 1733−1746.
(30) Laine, R. M. *J. Mater. Chem.* **2005**, *15*, 3725−3744.
(31) Zhang, L.; Abbenhuis, H. C. L.; Yang, Q. H.; Wang, Y. M.; Magusin, P. C. M. M.; Mezari, B.; Santen, R. A. v.; Li, C. *Angew. Chem., Int. Ed.* **2007**, *46*, 5003−5006.
(32) Roll, M. F.; Kampf, J. W.; Kim, Y.; Yi, E.; Laine, R. M. *J. Am. Chem. Soc.* **2010**, *132*, 10171−10183.
(33) Kim, Y.; Koh, K.; Roll, M. F.; Laine, R. M.; Matzger, A. J. *Macromolecules* **2010**, *43*, 6995−7000.
(34) Qin, Y. C.; Ren, H. B.; Zhu, F. H.; Zhang, L.; Shang, C. W.; Wei, Z. J.; Luo, M. M. *Eur. Polym. J.* **2011**, *47*, 853−860.
(35) Nischang, I.; Brüggemann, O.; Teasdale, I. *Angew. Chem., Int. Ed.* **2011**, *50*, 4592−4596.
(36) Alves, F.; Scholder, P.; Nischang, I. *ACS Appl. Mater. Interfaces* **2013**, *5*, 2517−2526.
(37) Morrison, J. J.; Love, C. J.; Manson, B. W.; Shannon, I. J.; Morris, R. E. *J. Mater. Chem.* **2002**, *12*, 3208−3212.
(38) Arslan, H. In *Block and Graft Copolymerization*; Ceresa, R. J., Ed.; Wiley: London, 1976.
(39) Hayashi, K.; Ono, K.; Suzuki, H.; Sawada, M.; Moriya, M.; Sakamoto, W.; Yogo, T. *Chem. Mater.* **2010**, *22*, 3768−3772.
(40) Tucker-Schwartz, A. K.; Farrell, R. A.; Garrell, R. L. *J. Am. Chem. Soc.* **2011**, *133*, 11026−11029.
(41) Yantasee, W.; Warner, C. L.; Sangvanich, T.; Addleman, R. S.; Carter, T. G.; Wiacek, R. J.; Fryxell, G. E.; Timchalk, C.; Warner, M. G. *Environ. Sci. Technol.* **2007**, *41*, 5114−5119.
(42) Kan, X. W.; Geng, Z. R.; Zhao, Y.; Wang, Z. L.; Zhu, J. J. *Nanotechnology* **2009**, *20*, 165601−165607.
(43) Li, X. L.; Li, Y. F.; Zhang, S. D.; Ye, Z. F. *Chem. Eng. J.* **2012**, *183*, 88−97.
(44) Faraji, M.; Yamini, Y.; Rezaee, M. *J. Iran. Chem. Soc.* **2010**, *7*, 1−37.
(45) Liu, Q. X.; Xu, Z. H. *Langmuir* **1995**, *11*, 4617−4622.
(46) Hao, Y. J.; Chong, Y. Z.; Li, S. R.; Yang, H. Q. *J. Phys. Chem. C* **2012**, *116*, 6512−6519.
(47) Peng, L.; Qin, P. F.; Lei, M.; Zeng, Q. R.; Song, H. J.; Yang, J.; Shao, J. H.; Liao, B. H.; Gu, J. D. *J. Hazard. Mater.* **2012**, *209−210*, 193−198.